Dislocation mechanics of copper and iron in high rate deformation tests

Ronald W. Armstrong,[1,a)] Werner Arnold,[2] and Frank J. Zerilli[3]
[1]*University of Maryland, College Park, Maryland 20742, USA*
[2]*MBDA-TDW, 86523 Schrobenhausen, Germany*
[3]*Department of Research and Technology, Naval Surface Warfare Center, Indian Head, Maryland 20640, USA*

(Received 9 August 2008; accepted 3 December 2008; published online xx xx xxxx)

Different dislocation processes are shown to be operative under high rate loading by impact-induced shock tests as compared with shockless isentropic compression experiments (ICEs). Under shock loading, the plastic deformation rate dependence of the flow stress of copper is attributed to dislocation generation at the propagating shock front, while in shockless ICEs, the rate dependence is attributed to drag-controlled mobile dislocation movement from within the originally resident dislocation density. In contrast with shock loading, shockless isentropic compression can lead to flow stress levels approaching the theoretical yield stress and dislocation velocities approaching the speed of sound. In iron, extensive shock measurements reported for plate impact tests are explained in terms of plasticity-control via the nucleation of deformation twins at the propagating shock front.
 [DOI: 10.1063/1.3067764]

I. INTRODUCTION

In the 1980s, Follansbee *et al.*[1] reported a strong upturn in the flow stress of copper, determined at 0.15 strain and 300 K, when tested at the upper end of higher strain rates achieved in split-Hopkinson pressure bar (SHPB) experiments. The resulting flow stress dependence is shown in Fig. 1. A number of other metals were observed to have similar upturns in flow stress at strain rates of the order of 10^4 s^{-1}.

Figure 1 also displays "asymptotes" for the low and high strain rate dependencies of the activation area for a thermally activated dislocation model for plastic flow. In the figure, the asymptotes are labeled with the limiting values of the activation area A^* determined from the expression

$$A^* = \frac{kT}{b}\left(\frac{\partial \ln \dot{\gamma}}{\partial \tau^*}\right)_T, \tag{1}$$

where k is Boltzmann's constant, T is absolute temperature, $b=0.255$ nm is the dislocation Burgers vector of copper, $\dot{\gamma}$ is the shear strain rate, and τ^* is the thermal component of shear stress.

For connection of Eq. (1) with the material parameters in Fig. 1, $\Delta\tau^*=\Delta\sigma/m$, $\dot{\varepsilon}=\dot{\gamma}/m$, and $m=3.08$ is the Taylor orientation factor relating single crystal shear stress and strain to the corresponding polycrystal effective stress and strain; see, for example, the thermal activation description for dislocation dynamics given by Armstrong.[2] In accordance with that model description of the polycrystal flow stress σ_ε at constant tensile or compressive strain ε,

$$\sigma_\varepsilon = m\tau = m(\tau^* + \tau_G + k_s\ell^{-1/2}), \tag{2}$$

where τ_G is an athermal shear stress that is dependent on the dislocation density and solute concentration, k_s is the so-called microstructural shear stress intensity for overcoming the grain boundary resistance, and ℓ is the polycrystal grain diameter.

As will be seen for iron, the slip-determined $k_\varepsilon=mk_s$ and a larger twinning-determined k_T play important roles in determining the initial yielding responses to shock loading. The evaluation of Eq. (2) at $\ell^{-1/2}=0$ is taken to specify the average dislocation friction stress $\sigma_0=m(\tau^*+\tau_G)$. Also for iron, the temperature and strain rate dependencies of σ_ε are in σ_0. Otherwise, as noted in Fig. 1 for copper, a relatively large value of $A^*\sim 1000b^2$, corresponding to $(\Delta\sigma/\Delta \ln \dot{\varepsilon})_T \sim 0.8$ MPa, is measured as a typical value for a face-centered-cubic (fcc) metal tested at conventional tensile or compressive strain rates, and such measurements are generally attributed to the thermally activated overcoming of dislocation intersections during the slip process.

In the present article we account for the strong upturn shown in Fig. 1 for the copper flow stress measurements by making connection on a dislocation nucleation basis with

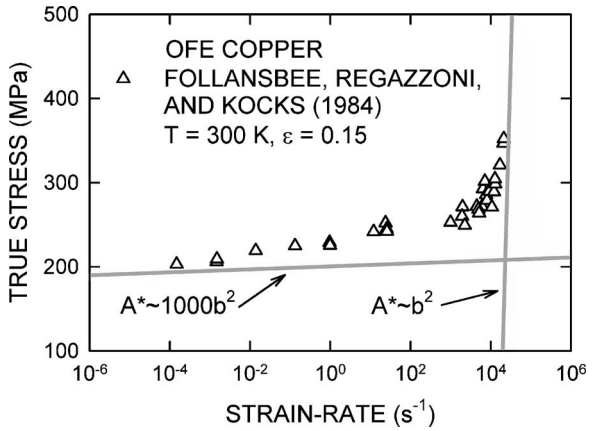

FIG. 1. The flow stress dependence on strain rate of oxygen-free electronic copper at 0.15 strain and 300 K as reported by Follansbee *et al.* (Ref. 1) and fitted with asymptotic activation area A^* values at the low and high strain rates.

a)Electronic mail: rona@umd.edu.

other sharply rising, shock-induced, plastic flow stresses measured both for copper by Swegle and Grady[3] and for iron by Arnold.[4] The upturn in the SHPB measurements of copper by Follansbee *et al.*[1] is shown to have provided early evidence pointing toward the substantially higher shock-induced plastic flow stress measurements reported by Swegle and Grady.[3] The result is attributed to a changeover from the often employed Orowan equation, for relation of $d\gamma/dt$ and the dislocation velocity v in

$$\frac{d\gamma}{dt} = \rho b v, \tag{3}$$

where ρ is the dislocation density to the alternative dislocation nucleation equation for $d\gamma/dt$, also obtained from Orowan[5] as

$$\frac{d\gamma}{dt} = \frac{d\rho}{dt} b \Delta x_d, \tag{4}$$

where $d\rho/dt$ is the rate of nucleation and Δx_d is a small distance associated with the nucleated dislocation displacement.

Arnold[4] measured the Hugoniot elastic limit (HEL) pressure and follow-on jump to a higher plastic flow pressure exhibited for plate impact experiments conducted on different grain-sized iron materials. The tests covered a wide range of projectile/target thicknesses. Comparison of the results with postshock metallographic observations and with the previously mentioned grain size dependencies for slip or deformation twinning in iron provides evidence for roles played by both deformation responses and transition between them in determining reasonably strong, although more so for twinning than slip, grain size dependences of the HEL. On the other hand, because a substantial shear strain is imposed at all points along a propagating shock front with consequent relaxation produced in iron by nanoscale twin nucleation, the higher shock-induced plastic flow stress will be shown to be unaffected by the material grain size.

Last but perhaps most interesting is an interpretation put forward for recent isentropic compression experiment (ICE) results reported for copper by Jarmakani *et al.*[6] No shock is produced in the uniform loading of an ICE test, and, therefore, the flow stress levels and dislocation velocities are shown to be limited only by the energy dissipation resulting from interaction of the moving dislocations with lattice vibrations, that is, the so-called influence of "phonon drag." Consequently, the flow stress may increase to the theoretical cohesive limit with velocities approaching the speed of sound. Quantitative evaluation of the results of Jarmakani *et al.*[6] leads to the conclusion that, at the highest peak pressure reported of ~52 GPa, the plastic flow stress is very near to the theoretical limit for copper.

II. CONVENTIONAL STRAIN RATE, SHPB, AND SHOCK RESULTS

A. Copper

Figure 2 shows over a larger range of stress than in Fig. 1 a comparison of the SHPB results from both Follansbee *et al.*[1] and the shock-induced plasticity results of Swegle and Grady.[3] At the relatively lower stresses shown for the SHPB results, the data follow a thermally activated dislocation mechanics based relationship proposed by Zerilli and Armstrong, as updated recently by Zerilli[7] in the fcc form

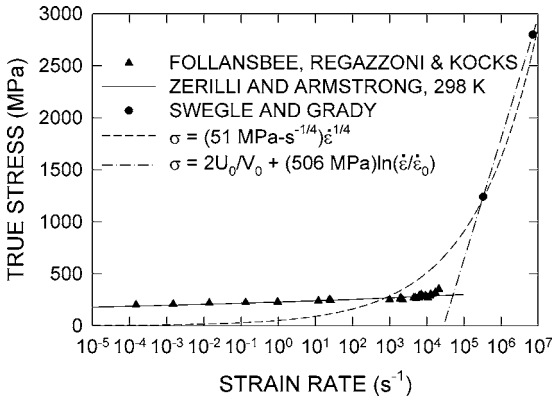

FIG. 2. Flow stress dependence on strain rate reported by Follansbee *et al.* (Ref. 1) (triangles) and shock-induced plasticity results reported by Swegle and Grady (Ref. 3) (circles), compared with ZA thermal activation model, the Swegle–Grady empirical relation, and the thermal activation dislocation nucleation model.

$$\sigma_\varepsilon = B_0 \varepsilon^{1/2} \exp(-(\beta_0 - \beta_1 \ln \dot{\varepsilon})T) + \sigma_G + k_\varepsilon \ell^{-1/2} \tag{5}$$

in which the experimental constants σ_G, B_0, β_0, β_1, and k_ε were determined from other experimental results. The first term on the right-hand side of Eq. (5) is $\sigma^* = m\tau^*$ in accordance with Eq. (2). The empirical relationship

$$\sigma \propto \dot{\varepsilon}^{1/4} \tag{6}$$

proposed by Swegle and Grady[3] is also shown in the figure as the dashed line passing through their pair of shock-induced plasticity measurements. The filled-black-circle stress values are transformed from the measured shock pressures P using the relation

$$\sigma = \frac{1-2\nu}{1-\nu} P, \tag{7}$$

where ν is Poisson's ratio. A value of Poisson's ratio $\nu = 0.345$ for copper was used.

Armstrong *et al.*[8] proposed that the boundary conditions at the propagating shock front required sequential generation of a nanoscale dislocation structure so that Orowan's second equation [Eq. (4) above] should be the appropriate relationship to employ in a thermal activation model. Further, as seen from the result shown in Fig. 1, a lower limiting value of the area of activation of order of $\sim b^2$ dimension applies. By incorporation of a lower limiting activation volume V_0, then in a thermally activated relationship for $d\rho/dt$, the simple relation is obtained

$$\sigma = \frac{2U_0}{V_0} - \frac{2kT}{V_0} \ln\left(\frac{\dot{\varepsilon}_0}{\dot{\varepsilon}}\right) \tag{8}$$

in which U_0 is the Gibbs free energy of activation in the absence of an applied shear stress and the constant $\dot{\varepsilon}_0$ is a reference upper-limiting strain rate. The flow stress in this case is seen to be linear in $\ln \dot{\varepsilon}$.

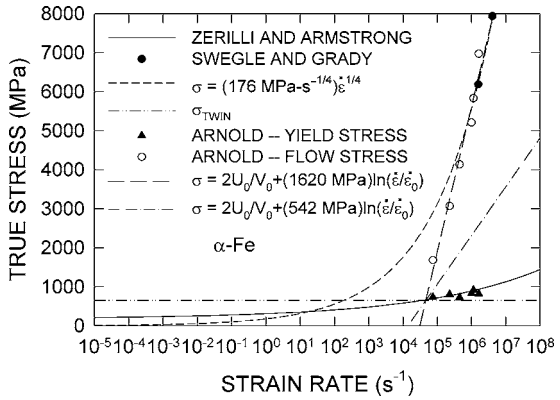

FIG. 3. HEL and shock-induced plastic flow stresses for ARMCO iron from Arnold (Ref. 4), in comparison with a number of relationships proposed to fit either slip or deformation twinning aspects of the strain rate dependent behaviors.

Equation (8) is plotted in Fig. 2, with $V_0=A^*b$ taken as b^3 to give $2kT/V_0=506$ MPa at 300 K. The modeled quantity $2U_0/V_0$ is the theoretical limiting stress for dislocation nucleation and a reasonable order of magnitude estimate of ~5.8 GPa was assumed, giving a value of $\dot{\varepsilon}_0 \sim 2.3 \times 10^9$ s^{-1}. It is evident from an inspection of Fig. 2 that the data points of Follansbee *et al.*[1] and of Swegle and Grady[3] indicate a smooth transition from thermally activated dislocation motion to thermally activated dislocation generation.

B. Iron

Much information is available on the shock-induced deformation properties of ARMCO iron (first produced in 1909 by the American Rolling Mill Co., ARMCO ingot iron became the synonym for the purest steel-mill-produced iron, having a purity of more than 99% iron and especially including very low carbon content) that has been employed historically also, as a standard for equation of state studies, particularly relating to the determination by Bancroft *et al.*[9] of a shock pressure of 13.2 GPa for the (bcc) alpha-to-epsilon (hexagonal close packed) phase transformation. Although previous shock-induced deformation results were reported for iron in several pioneering investigations conducted at a single grain size, Arnold[4] investigated the shock-induced deformation properties for ARMCO material with the different average grain diameters of 20, 40, 80, and 400 μm, and, as mentioned, tested in plate impacts covering a large range of projectile and target thicknesses mostly centered on a thickness ratio of 1/2 for added determination of the material spallation properties. In Fig. 3, HEL (closed-triangle) and shock jump plasticity (open-circle) measurements are shown for the 80 μm grain size material that was extensively tested, for example, in this case at an intermediate thickness ratio of 3/6 (in millimeter thicknesses), respectively, for the impacting plate and specimen. Again, the shock pressures have been transformed to effective shear stress measurements according to Eq. (7) but with $\nu=0.288$ for iron. Excellent agreement is shown between the open-circle points of Arnold[4] and the pair of filled-circle measurements reported by Swegle and Grady.[3]

A comparison in Fig. 3 of the power law ($\dot{\varepsilon}^{1/4}$) and linear ($\ln \dot{\varepsilon}$) dependence given by Eq. (8) favors the latter description. Nevertheless, model evaluation in this case of the slope of the linear dependence on $\ln \dot{\varepsilon}$ in Eq. (8), with $V_0=b^3$ and $b=0.248$ nm for slip in bcc iron, gives the dot-dashed line of lower slope that is shown in the figure; the slope is approximately three times lower than the fitted long-dashed line through the combined Arnold[4] and Swegle and Grady[3] data. Armstrong *et al.*[8] accounted for the steeper slope of the shock-induced plasticity results in Fig. 3, corresponding to employment of $V_0=(b^3/3)$, by proposing that the propagating shock front was nucleating a nanoscale structure of deformation twins, with $V_0=b_T^2 b$ and $b_T=2(a/6)$ [111] for a smallest two-layer twin thickness;[10] a is the crystal unit cell lattice parameter. Postshock metallographic observations made on Arnold's 80 μm grain size material showed significant deformation twinning for shock pressures greater than ~3 GPa, corresponding to $\sigma > \sim 1.8$ GPa, thus providing evidence for significant residual microscale twinning associated with all of the open circle points.

III. SLIP/TWINNING TRANSITION AT THE HUGONIOT ELASTIC LIMIT IN IRON

An interesting comparison of predicted slip and deformation twinning stresses also is indicated at the lower level of stress in Fig. 3 for the closed-triangle σ values obtained from Arnold's HEL measurements. In the figure, the horizontal double-dot-dashed line prediction was obtained for the twinning stress σ_T from the equation

$$\sigma_T = \sigma_{T0} + k_T \ell^{-1/2} \quad (9)$$

in which $\sigma_{T0}=330$ MPa and $k_T=90$ MPa $mm^{1/2}$ as determined from other results reported for ARMCO iron and low carbon steel materials,[11] whereas the Zerilli and Armstrong (ZA) curve, that is also shown in the figure, applies for slip-controlled deformation as computed with the bcc-type equation[7]

$$\sigma = B \exp(-\beta T) + A\varepsilon^n + \sigma_G + k_y \ell^{-1/2}, \quad (10)$$

in which $\beta=\beta_0-\beta_1 \ln \dot{\varepsilon}$ and σ_G, B, β_0, β_1, A, n, and k_y were taken from earlier reported experimental constants determined for other results.[12] The indication from the compared relationships and the HEL-transformed (closed-triangle) measurements is that the 80 μm grain size material may have initially yielded by slip but only just so because twinning occurred soon after deformation began, as definitely established via postshock metallographic observations made for the higher open-circle flow stress results.[4]

The competition between slip and deformation twinning in iron and other bcc metals is a well-known consideration in accounting for deformation stress levels measured at low temperatures or high strain rates near to those required for cleavage fracturing. Therefore, it seemed worthwhile to re-examine the total HEL and flow stress measurements reported by Arnold[4] for the 80 μm grain size material, as shown in Fig. 4. The figure legend includes the full range of projectile/target thicknesses that were employed in the tests and shows the dependencies of the four constitutive equations that have been described above; σ_{SG} is for the Swegle

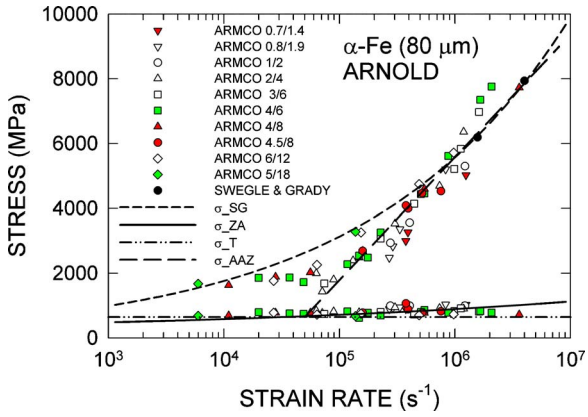

FIG. 4. (Color online) A comprehensive listing of shock-induced HEL and plastic flow stresses for ARMCO iron at different projectile/target thicknesses from Arnold (Ref. 4), in comparison with a number of relationships proposed to fit either slip or deformation twinning aspects of the strain rate dependent behaviors.

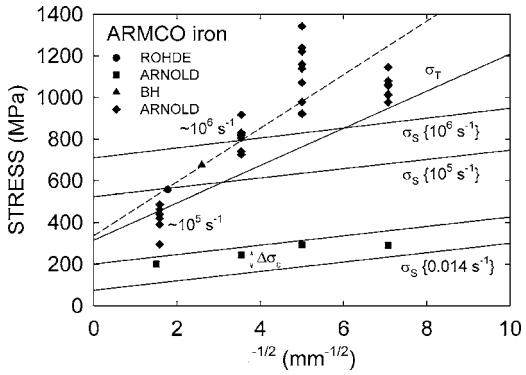

FIG. 5. Preshock hardness and shock flow stress measurements, both from Arnold (Ref. 4), along with shock measurements from Rohde (Ref. 13) and Barker and Hollenbach (Ref. 14) plotted against inverse square root of grain size for both slip and deformation twinning.

and Grady power law relation and σ_{AAZ} is the thermally activated dislocation generation relation, Eq. (8).

To some extent, the distinctions made reasonably clearly in Fig. 3 are now blurred by the variations shown among the greater number of experimental results. On the expanded abscissa scale covering a range of strain rates between $\sim 6 \times 10^3$ and $\sim 4.5 \times 10^6$ s^{-1}, the lower HEL σ values appear to follow the computed twinning stress level at first but then move a little bit upwards at the higher strain rates to the calculated slip stress dependence that is indicated in Fig. 3. The same linear in $\ln \dot{\varepsilon}$ dependence of the higher shock-induced plastic flow stress measurements from Fig. 3 is drawn in Fig. 4 as the long-dashed line, and the previously described data are also shown to be buried in the total band of the higher distributed measurements. Close examination of the higher distributed stress values shows, at the lower strain rates, that the shock-induced flow stress jumps to a relatively constant plasticity level and persists so over an approximate order-of-magnitude increase in strain rate. Thereafter, with reasonable variations, the shock-induced plastic flow stresses follow the linear in $\ln \dot{\varepsilon}$ dependence previously described with Eq. (8).

IV. GRAIN SIZE DEPENDENT HUGONIOT ELASTIC LIMIT

Despite the close relationship of the slip and twinning stress measurements shown in Fig. 4 for the 80 μm grain size material, the competition between the two deformation mechanisms is strongly influenced by the material grain size, for example, as evidenced in the comparison of predictions from Eqs. (9) and (10), and particularly involving the different magnitudes of the microstructural stress intensity, for example, of $k_T = 90$ MPa $\text{mm}^{1/2}$ for deformation twinning[11] as compared with a slip-controlled yield stress value of $k_y = 22$ MPa $\text{mm}^{1/2}$; a lesser value of $k_\varepsilon = 5$ MPa $\text{mm}^{1/2}$ applies for copper.[11,12]

Assessment of the relatively more important grain size influences on the iron HEL σ values, therefore, is shown next on a polycrystal reciprocal square root of grain diameter basis in Fig. 5 for both the slip σ_S and twinning σ_T stress dependencies. Individual HEL σ values obtained from earlier pioneering investigations made by Rohde[13] and by Barker and Hollenbach[14] are included in the figure. The importance of a thermally activated τ^* in Eqs. (2) and (10) is made clear by the increasing intercept friction stresses obtained for the σ_S lines evaluated at the differently labeled strain rates. For σ_T, a solid line of correspondingly higher k_T was obtained from Eq. (9), and also a dashed line is shown for a possibly raised σ_T at the higher shock-imposed loading rates. The slip versus twinning issue for iron had been assessed previously on this same grain size basis for ARMCO iron SHPB results[15] and for the current material grain sizes subjected to Taylor solid cylinder impact tests.[16]

Consider first in Fig. 5 the lower filled-square points that are shown to follow an approximate σ_S-type dependence. These points were obtained from diamond pyramid hardness measurements made by Arnold[4] on the different grain size materials before shocking. For the purpose of Fig. 5, the individual hardness measurements were divided by a factor of 3 to represent the material flow stress at a strain value of 0.075. In turn, the lowest σ_S linear dependence shown for a conventional strain rate of 0.014 s^{-1} was raised by $\Delta\sigma_\varepsilon = A\varepsilon^n$ for $\varepsilon = 0.075$ by employing the previous iron constants A and n mentioned[12] for Eq. (10). Thus, the raised line passing just above the converted hardness points was obtained. Reasonable agreement is taken to be shown by the converted data points and the slip comparison.

Next, attention is turned to the higher filled diamond points for Arnold's converted HEL σ measurements that were obtained at different grain sizes but at the same 3/6 projectile/target ratio. These data, which are vertically spread over a range in stress at each grain size, are associated with different strain rates, also, as indicated at the left-side two larger grain diameter cases of 400 and 80 μm with values of $\dot{\varepsilon} \sim 10^5$ and 10^6 s^{-1}. Note that the two higher σ_S lines are at the same pair of strain rates. Rohde[13] estimated that his filled circle point was obtained at a strain rate equaling 10^5 s^{-1}. In the Fig. 5 intersection of slip and twinning lines at the higher strain rate, then, the 80 μm grain size material is seen to be very near to the predicted transition from slip-controlled plastic flow at smaller grain size and twinning-controlled deformation at larger grain size, particularly, if a higher twin-

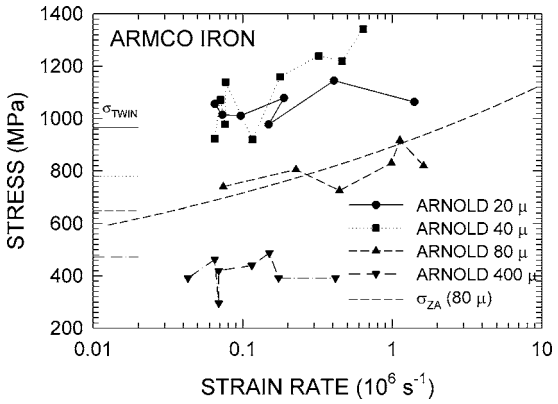

FIG. 6. The strain rate dependence of the HEL yield stresses of ARMCO iron at different grain sizes, from Arnold (Ref. 4), compared with estimated twinning stress levels and, for a grain size of 80 μm, with the bcc ZA slip-type equation (Ref. 7).

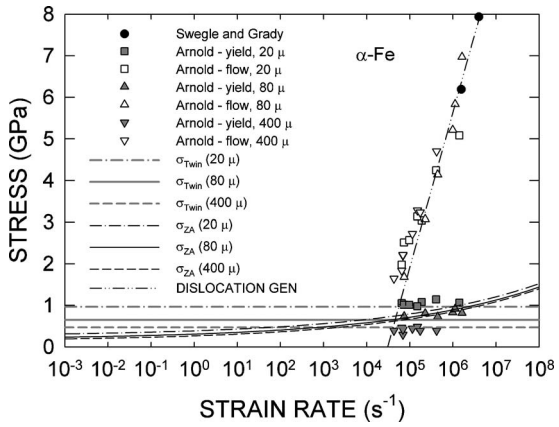

FIG. 7. The HEL and shock stresses for ARMCO iron of different grain sizes, from Arnold (Ref. 4), in comparison with the differently modeled slip, deformation twinning, and twin nucleation stress predictions.

ning (dashed-line) stress dependence may be operable at these greater strain rates. Armstrong and Worthington[17] previously reported a model for deformation twinning that predicted a relatively small strain rate dependence of σ_T.

There is also indication in Fig. 5 of the smaller 40 and 20 μm grain size materials possibly following a σ_S dependence for slip. In this way the measurements would be following the well-known increasing tendency for slip to be rate controlling at finer grain sizes. Figure 6, in showing details of the strain rate dependence, appears at first sight to confirm the indication. In Fig. 6, the abscissa strain rate scale is spread larger to show the HEL σ measurements for the four grain size materials at the respective plastic strain rates determined for the higher shock propagation stresses. The computed twinning stresses from Eq. (9) are marked along the ordinate scale. The relative strain rate independence of the 400 μm grain size material and the level of the stress values compared to the twinning stress marker both are in agreement with the HEL being fully controlled by deformation twinning. The dashed curve through the 80 μm material results is that computed with Eq. (10) by employing the previously determined constants. Agreement is shown with a slip-controlled HEL σ but the determined stress levels, as indicated earlier, occur above the predicted twinning stress level. Here the indication is that the 80 μm material is in the transition region where slip and twinning may be equally preferred but the measured σ values are principally determined by slip. The 40 and 20 μm grain size materials also appear to follow a slip-type strain rate dependence for the HEL σ but their being higher than the predicted twinning stress level cannot be accounted for by the slip-controlled grain size dependence with k_y=22 MPa mm$^{1/2}$, as shown in Fig. 7.

V. GRAIN SIZE INDEPENDENT SHOCK-INDUCED PLASTIC FLOW STRESS

Several models have been proposed for dislocation nucleation at a propagating shock front beginning from the pioneering description of shock induced deformations described by Smith.[18–21] A main consideration in determining the need for dislocation (or twin) nucleation is that the large magnitude of the locally imposed shear strains at all points along a propagating shock front are too large to be relieved by the displacement of the few dislocation line segments contained in, or crossing, the front or by the remote displacement of the resident dislocation density behind the front. The intersection of grain boundaries with the shock front is an even rarer occurrence and thus, the material grain size should not be a significant factor in determining the shock-induced plastic deformation rate. The model consideration is in agreement with the results shown in Fig. 7 for iron of 400, 80, and 20 μm grain size, all tested at 3 to 6 mm projectile/target thicknesses.

In the lower part of Fig. 7, the just-discussed HEL stress values for each grain size are plotted in comparison with both Eqs. (9) and (10) predictions; the 40 μm grain size results are omitted from the figure for clarity. As can be seen at this dimensional scale, except for the 80 μm grain size material results, the emphasis would be on a twinning explanation for the HEL stress and, as mentioned above, the different grain size predictions for slip control are shown to be too small to account for the results. The greater interest in Fig. 7, however, is in the apparent grain size independence of the shock-induced plastic flow stresses at all of the grain sizes. The double-dot-dashed line is the same one drawn in Fig. 3 for the twin nucleation relationship given in Eq. (8). The result provides confirmation of the previously referenced shock model descriptions.

VI. ISENTROPIC COMPRESSION OF COPPER

As mentioned in Sec. I, the uniform pressure buildup in isentropic compression provides for the possibility of reaching a high plastic flow stress and corresponding high plastic strain rate in shockless loading. Jarmakani *et al.*[6] reported quasi-isentropic compression experiments performed with a two-stage gas gun employing functionally graded impacters applied to [001]-oriented copper crystals sustaining pressures ranging between 17.7 and 51.5 GPa.

Figure 8 shows the effective shear stress measurements, achieved again via transformation with Eq. (7), for test results involving either zero hold time (short) (open-squares) or 10 μs. (long) (filled-square) pressure pulses. The stress

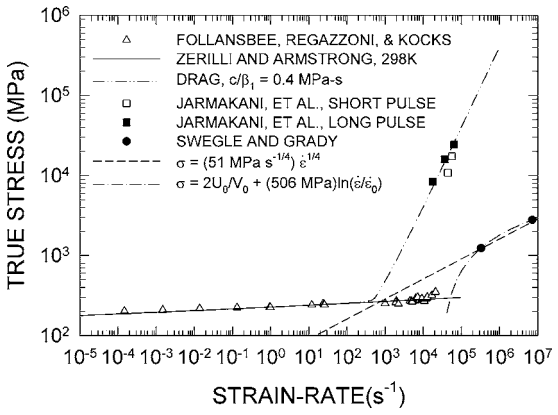

FIG. 8. A comparison for copper of Hopkinson bar, shock, and isentropic compression stresses (Refs. 1, 3, and 6, respectively) as a function of strain rate and fitted with the proposed empirical and model constitutive relationships proposed for the respective strain rate regimes.

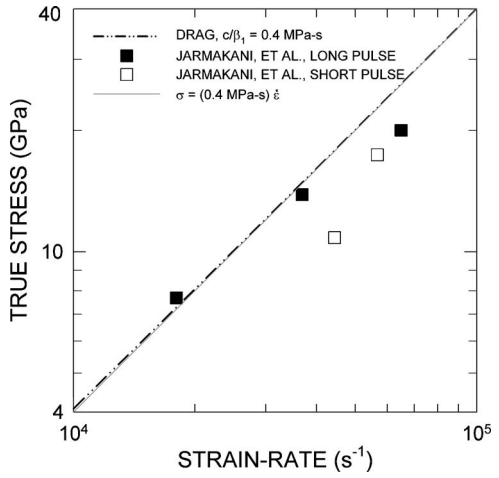

FIG. 9. ICE results for copper, after Jarmakani *et al.* (Ref. 6), as a function of strain rate, showing linear stress dependence on strain rate in accordance with model prediction for drag-controlled slip (Ref. 24).

values are significantly higher than those in Fig. 2 but, perhaps surprisingly, the plastic strain rates are lower by one to two orders of magnitude. For comparison, the previously described shock results for copper from Fig. 2 are included in Fig. 8.

Jarmakani *et al.*[6] reported that an amount of deformation twinning, normally not a major concern in the high rate testing of copper except at the highest loading rates, was detected in post-ICE transmission electron microscope (TEM) examinations of the specimens tested at the two highest pressures. As evident in Fig. 8, the authors commented that their results did not follow the Swegle–Grady relationship for shocking of copper; rather the issue of a slip-twinning transition was explored via a Preston–Tonks–Wallace (PTW) constitutive equation[22] to compare estimations of critical pressures for twinning in both shock and ICE regimes. Remington *et al.*[23] provided a comparison of similar constitutive predictions made both by PTW and ZA equations applied to the high rate deformation of tantalum material; see their Fig. 1(b). Also, it is notable that the Jarmakani *et al.*[6] TEM observations were interpreted to show production of fewer dislocations in the post-ICE test specimens.

In Fig. 9, rather than consideration of a transition from slip to twinning, focus is directed to the experimental linear dependence of σ on the direct strain rate. In a previous report,[24] it was proposed that the ICE and shock tests are fundamentally different in that Orowan's Eq. (4) for dislocation generation is operative for the shock case, as discussed above for both copper and iron results, but under the shockless loading condition in isentropic compression, the strain rate is carried by the movement of mobile dislocations activated within the resident dislocation density described by Orowan's Eq. (3). The additional complication in this case is that with a dislocation density of, say, $\sim 10^7$ cm^{-2} and $b = 0.255$ nm, the average dislocation velocity at a shear strain rate of $\sim 5 \times 10^4$ s^{-1} would be ~ 2000 m/s, compared to an elastic shear wave speed of ~ 2900 m/s. The estimated dislocation velocity is too large to neglect the drag force on dislocations during their movement between thermal obstacles in the normal thermal activation description.

Previously, Zerilli and Armstrong[25] incorporated dislocation drag into a thermal activation model based on Orowan's Eq. (3) as part of an investigation leading to added drag resistance being a discounted option for explaining the upturn in the SHPB flow stresses shown in Fig. 1. From the previous investigation, the equation for a thermal component of effective shear stress including drag resistance is

$$\sigma^* = B \exp(-\beta T)\left(1 - \frac{c\dot{\varepsilon}}{\beta_1 \sigma^*}\right)^{-\beta_1 T}, \tag{11}$$

where

$$c = c_0 m^2 \beta_1 / \rho b^2 \tag{12}$$

is a constant and c_0 is the drag coefficient defined by the equation

$$b\tau = c_0 v, \tag{13}$$

where $b\tau$ is the force per unit length of dislocation line. Equation (11) is an implicit equation for σ^*. In the high strain rate limit, the solution reduces to

$$\sigma^* = \frac{c}{\beta_1}\dot{\varepsilon}. \tag{14}$$

A value of $c/\beta_1 = c_0 m^2/\rho b^2 \approx 0.4$ MPa s is shown in Fig. 8 to fit the Jarmakani *et al.*[6] data. The exact solution for Eq. (11) is shown as the dash-double-dot line in both Figs. 8 and 9. In the expanded scale of Fig. 9, the linear relation, Eq. (14), is plotted as the light solid line, which, in the region of strain rates of the experimental data, is seen to be nearly indistinguishable from the exact solution.

Determination of the drag coefficient from the linear slope in Fig. 9 requires an estimation of the dislocation density, which can be made from Orowan's Eq. (3). In term of the effective strain rate, Eq. (3) becomes

$$\dot{\varepsilon} = \frac{\rho b}{m} v. \tag{15}$$

The upper limit to the dislocation velocity is the shear wave speed. Taking the value of shear wave speed for copper to be 2900 m/s and a strain rate value $\dot{\varepsilon} \approx 7 \times 10^4$ s^{-1} correspond-

ing to the highest strain rate data point of Jarmakani *et al.*,[6] then, from Eq. (15), a value of $\rho \approx 2.9 \times 10^7$ cm^{-2} is determined. The value is low but not unreasonable for the mobile dislocation density. With this value of ρ, using Eq. (12), the estimated drag coefficient $c_0 \approx 8 \times 10^{-4}$ Pa s.

Lastly, there is the issue of comparing the foregoing drag coefficient to experimental values that have been reported previously for the movement of individual dislocations, generally, at orders of magnitude lower stress levels. Jassby and Vreeland[26] reported such drag coefficient measurements for copper to be in the range of 1×10^{-5} to 8×10^{-5} Pa s. Their own measurement gave a value of 1.7×10^{-5} Pa s at 296 K. The value calculated here exceeds the reported values by at least an order of magnitude. However it is well known that as the elastic shear wave velocity is approached, the dislocation drag coefficient should increase without bound, becoming infinite at the shear wave speed (for example, see De Hosson *et al.*[27]). Thus, the present result is quite consistent with the idea that, at the highest strain rates achieved by Jarmakani *et al.*,[6] mobile dislocation velocities are approaching the shear wave speed with flow stresses due to drag approaching the theoretical yield stress limit for velocity control.

VII. CONCLUSION

The strain rate dependence of the flow stress of copper has been tracked over a very large range from $\sim 10^{-4}$ to nearly 10^7 s^{-1}. Along the way, a number of different dislocation mechanics-based mechanisms have been associated with the measurements, for example, of dislocation intersections at conventional tension or compression measurements, of transition at the high end of SHPB measurements to dislocation nucleation that is shown to be rate controlling for impact-induced shock wave propagation, and lastly, of ICE-type drag-controlled very high dislocation velocities being operative at exceptionally high stresses.

For the higher ICE results displayed in Fig. 8, deviations from the normal thermal activation flow stress due to drag begin appearing at strain rates as low as 500 s^{-1} and become significant by 1000 s^{-1}. On the other hand, the lower stress dislocation generation control shown for the shock cases in Figs. 2–7 tends to limit the increase in flow stress to smaller values characteristic of an increased dislocation density and defers any possible influence of drag to higher imposed strain rates.

Finally, the strain rate dependence of the HEL yield stress of iron of different grain sizes tested in plate impact tests has been accounted for in terms of competition between alternative grain-size-dependent slip and twinning deformation responses but followed by grain-size-independent shock-induced plasticity controlled by the nucleation of deformation twins. The thermal activation areas determined from the strain rate sensitivity $(\Delta\sigma/\Delta \ln \dot{\varepsilon})_T$, as evaluated for twin nucleation in ARMCO iron and for slip nucleation in shocked copper, are importantly attributed to needed mechanisms of relief of the very large strains imposed at all points along a propagating shock front.

[1] P. S. Follansbee, G. Regazzoni, and U. F. Kocks, in *Mechanical Properties of Materials at High Strain Rates*, edited by J. Harding (Institute of Physics, London, 1984), p. 71.
[2] R. W. Armstrong, J. Sci. Ind. Res. **32**, 591 (1973).
[3] J. W. Swegle and D. E. Grady, J. Appl. Phys. **58**, 692 (1985).
[4] W. Arnold, *Dynamisches Werkstoffverhalten von Armco-Eisen bei Stosswellenbelastung* (VDI-Verlag, Duesseldorf, 1992).
[5] E. Orowan, Proc. Phys. Soc. London **52**, 8 (1940).
[6] H. Jarmakani, J. M. McNaney, B. Kad, D. Orlikowski, J. H. Nguyen, and M. A. Meyers, Mater. Sci. Eng., A **463**, 249 (2007).
[7] F. J. Zerilli, Metall. Mater. Trans. A **35**, 2547 (2004).
[8] R. W. Armstrong, W. Arnold, and F. J. Zerilli, Metall. Mater. Trans. A **38**, 2605 (2007).
[9] D. Bancroft, E. L. Peterson, and S. Minshall, J. Appl. Phys. **27**, 291 (1956).
[10] R. W. Armstrong and F. J. Zerilli, in *Advances in Twinning*, edited by S. Ankem and C. S. Pande (TMS, Warrendale, 1999), p. 67.
[11] F. J. Zerilli and R. W. Armstrong, in *Shock Waves in Condensed Matter*, edited by S. C. Schmidt and N. C. Holmes (Elsevier Science, New York, 1987), p. 273.
[12] F. J. Zerilli and R. W. Armstrong, J. Appl. Phys. **61**, 1816 (1987).
[13] R. W. Rohde, Acta Metall. **17**, 353 (1969).
[14] L. M. Barker and R. E. Hollenbach, J. Appl. Phys. **45**, 4872 (1974).
[15] R. W. Armstrong and F. J. Zerilli, J. Phys. **49**, (C3), 529 (1988).
[16] H. Nahme, M. Hitl, and W. Arnold, in *Shock Compression of Condensed Matter*, edited by S. C. Schmidt and W. C. Tao (American Institute of Physics, New York, 1995), p. 619.
[17] R. W. Armstrong and P. J. Worthington, in *Metallurgical Effects at High Strain Rates*, edited by R. W. Rhode, B. M. Butcher, and J. R. Holland (Plenum, New York, 1973), p. 401.
[18] C. S. Smith, Trans. Am. Inst. Min., Metall. Pet. Eng. **212**, 574 (1958).
[19] M. A. Meyers, Scr. Metall. **12**, 21 (1978).
[20] F. A. Bandak, R. W. Armstrong, and A. S. Douglas, Phys. Rev. B **46**, 3228 (1992).
[21] F. A. Bandak, D. H. Tsai, R. W. Armstrong, and A. S. Douglas, Phys. Rev. B **47**, 11681 (1993).
[22] D. L. Preston, D. L. Tonks, and D. C. Wallace, J. Appl. Phys. **93**, 211 (2003).
[23] B. A. Remington, P. Allen, E. M. Bringa, J. Hawreliak, D. Ho, K. T. Lorenz, H. Lorenzana, J. M. McNaney, M. A. Meyers, S. W. Pollaine, K. Rosolankova, B. Sadik, M. S. Schneider, D. Swift, J. Wark, and B. Yaakobi, Mater. Sci. Technol. **22**, 474 (2006).
[24] R. W. Armstrong, W. Arnold, and F. J. Zerilli, *Shock Compression of Condensed Matter—2007*, edited by M. Elert, M. D. Furnish, R. Chau, N. C. Holmes, and J. H. Nguyen (American Institute of Physics, New York, 2007), p. 623.
[25] F. J. Zerilli and R. W. Armstrong, Acta Mater. **40**, 1803 (1992).
[26] K. M. Jassby and T. Vreeland, Jr., Philos. Mag. **21**, 1147 (1970).
[27] J. Th. De Hosson, A. Roos, and E. D. Metselaar, Philos. Mag. **81**, 1099 (2001).